HHS Public Access

Author manuscript

Magn Reson Med. Author manuscript; available in PMC 2021 April 01.

Published in final edited form as:

Magn Reson Med. 2020 October ; 84(4): 2088–2102. doi:10.1002/mrm.28250.

Impact of age, sex, and global function on normal aortic hemodynamics

Michael B. Scott[1,2], **Hyungkyu Huh**[1], **Pim van Ooij**[3], **Vincent Chen**[1], **Brenda Herrera**[1], **Mohammed Elbaz**[1], **Patrick McCarthy**[4,5], **S. Chris Malaisrie**[4,5], **James Carr**[1], **Paul W. M. Fedak**[5,6], **Michael Markl**[1,2], **Alex J. Barker**[7]

[1]Department of Radiology, Feinberg School of Medicine, Northwestern University, Chicago, IL, USA [2]Department of Biomedical Engineering, McCormick School of Engineering, Northwestern University, Evanston, IL, USA [3]Department of Radiology and Nuclear Medicine, Academic Medical Centre, Amsterdam, the Netherlands [4]Bluhm Cardiovascular Institute, Northwestern University Feinberg School of Medicine, Chicago, IL, USA [5]Division of Cardiac Surgery, Northwestern University Feinberg School of Medicine, Chicago, IL, USA [6]Department of Cardiac Sciences, University of Calgary, Calgary, AB, Canada [7]Department of Radiology, University of Colorado, Anschutz Medical Campus, Aurora, CO, USA

Abstract

Purpose: To examine the effects of age, sex, and left ventricular global function on velocity, helicity, and 3D wall shear stress (3D-WSS) in the aorta of $N = 100$ healthy controls.

Methods: Fifty female and 50 male volunteers with no history of cardiovascular disease, with 10 volunteers per age group (18–30, 31–40, 41–50, 51–60, and 61–80 years) underwent aortic 4D-flow MRI. Quantification of systolic aortic peak velocity, helicity, and 3D-WSS distribution and the calculation of age group–averaged peak systolic velocity and 3D-WSS maps ("atlases") were computed. Age-related and sex-related changes in peak velocity, helicity, and 3D-WSS were computed and correlated with standard metrics of left ventricular function derived from short-axis cine MRI.

Results: No significant differences were found in peak systolic velocity or 3D-WSS based on sex except for the 18- to 30-year-old group (males 8% higher velocity volume and 3D-WSS surface area). Between successively older groups, systolic velocity decreased (13%, <1%, 7%, and 55% of the aorta volume) and 3D-WSS decreased (21%, 2%, 30%, and 62% of the aorta surface area). Mean velocity, mean 3D-3D-WSS, and median helicity increased with cardiac output ($r = 0.27$–0.43, all $P < .01$), and mean velocity and 3D-WSS decreased with increasing diameter ($r > 0.35$, $P < .001$). Arch and descending aorta systolic mean velocity, mean 3D-WSS, and median helicity increased with normalized left ventricular volumes: end diastolic volume ($r = 0.31$–0.37, $P < .01$), end systolic volume ($r = 0.27$–0.35, $P < .01$), and stroke volume ($r = 0.28$–0.35, $P < .01$).

Correspondence: Alex J. Barker, Department of Radiology, Children's Hospital Colorado, 13123 E. 16th Ave. B125, Aurora, CO 80045, USA. alexander.barker@cuanschutz.edu.

SUPPORTING INFORMATION

Additional Supporting Information may be found online in the Supporting Information section.

Conclusion: Healthy aortic hemodynamics are dependent on subject age, and correlate with vessel diameter and cardiac function.

Keywords

4D flow MRI; aortic disease; flow imaging; healthy controls; hemodynamics

1 | INTRODUCTION

Cardiac MRI is used widely to risk-stratify and monitor cardiovascular disease. For example, left-ventricular volumes and transvalvular blood velocities are used to monitor the progression of aortic valve disease and its impact on myocardial function. However, a known challenge when using these values for risk stratification is their age and sex dependence. Large cohort studies have investigated left ventricular global function values and found significant variation in healthy controls as a function of both age and sex.[1–3] With recent technological advances, 4D-flow MRI (time-resolved 3D phase-contrast MRI with 3D velocity encoding)[4–6] is poised to complement existing cardiovascular MRI techniques with comprehensive blood-flow measurements available within a clinically feasible scan time and workflow. For instance, the technique allows for regional and maximum velocities to be comprehensively measured in entire volumes of interest.[7] In addition, more advanced parameters such as 3D wall shear stress (3D-WSS, calculated over the entire surface of the aorta from 3D velocity data) can be estimated, which is known to play a role in atherosclerosis,[8] and correlate with severity of aortopathy as defined by areas of extracellular matrix dysregulation and elastic fiber degeneration.[9]

However, less is known about the dependence of normal ranges as a function of sex and age for hemodynamic markers derived from 4D-flow MRI. A study in $N = 247$ subjects without aortic or aortic valve pathology showed significant decreases in peak velocity, helicity, and vorticity, as well as increases in aortic diameter with age measured on six planes in the thoracic aorta.[10] Previous work has investigated the use of healthy controls and registration tools developed for brain imaging, to form spatially resolved aortic “atlases” representing the group-averaged velocities and 3D-WSS distribution.[11,12] Velocity and 3D-WSS distributions in individual patients could then be compared with the healthy atlas values to identify regions where patients exceed specific confidence intervals (eg, 95% confidence intervals) for normal physiologic values. This approach has been used to investigate 3D-WSS-based extracellular matrix remodeling in the presence of valve disease.[9] However, subsequent work has indicated that 3D-WSS appears to vary with age; thus, a need exists to understand normal variations of physiology in healthy control groups, systematically stratified by age and sex.[13,14] Establishing a modality-specific set of 3D-WSS normal values from 4D-flow MRI is important, because 3D-WSS tends to be underestimated due to limited spatial resolution, segmentation variation, intravoxel dephasing, partial-volume effects, and lower velocity-to-noise ratio near the vessel wall. Finally, the effect of normal global cardiac function variations on the measurement of aortic hemodynamics, such as systolic velocity, 3D-WSS and helicity, has not been systematically investigated, and may be important to normalizing 4D-flow-derived hemodynamic quantities for comparison among individuals with varying cardiac function.

In this study, we aim to establish baseline normal values for velocity, 3D-WSS, and helicity distribution in 100 healthy controls across a wide range of ages and equally distributed for male and female sex. We present a comprehensive analysis of both age-dependent and sex-dependant-dependent 3D hemodynamics (velocity, helicity, 3D-WSS), along with their relationship to left-ventricular volumes, myocardial mass, and function (eg, ejection fraction, stroke volume). These data enable the comparison of a single patient with aortic pathology to age-matched and sex-matched groups of normal controls to identify regions of abnormal velocity and 3D-WSS for risk stratification studies. We hypothesize that normal values of aortic systolic velocity, helicity, and 3D-WSS distribution change with the age and sex of the subjects, and that the velocity, helicity, and 3D-WSS in the aorta are correlated to markers of left-ventricular function.

2 | METHODS

2.1 | Study population

A total of 111 subjects were prospectively enrolled for this internal review board–approved study. Of those enrolled, 11 were excluded because of incomplete data or poor data quality ($N = 3$), history of cardiovascular disease unreported at the time of recruitment ($N = 2$ arrhythmia, $N = 2$ mitral valve disease, $N = 1$ rheumatic heart disease, $N = 1$ history of congestive heart failure), or because of left-ventricular hypertrophy detected during analysis ($N = 2$). Left-ventricular hypertrophy was defined as a left-ventricular myocardial mass of more than 115 g/m^2 (males) or more than 95 g/m^2 (females).[15] The final analysis included 100 subjects, 10 male, and 10 female subjects per age group of 18–30 years, 31–40 years, 41–50 years, 51–60 years, and 61–80 years. Exclusion criteria included a self-reported history of cardiovascular disease, body mass index greater than 40 kg/m^2, claustrophobia, or evidence of cardiovascular disease following image review. The demographics of the study subjects are given in Table 1. The study was approved by the Northwestern University Institutional Review Board. All subjects provided informed, written consent.

2.2 | Magnetic resonance imaging

Magnetic resonance imaging was performed on 1.5T and 3T scanners (Aera, Skyra; Siemens, Erlangen, Germany). Each subject underwent a standard-of-care thoracic cardiovascular MRI to evaluate left-ventricular function and valve morphology. Each subject also had a 4D-flow MRI with sagittal-oblique coverage of the thoracic aorta, using prospective electrocardiographic gating during free breathing with a respiratory navigator on the lung–liver interface.[16] Four-dimensional-flow MRI data were acquired with spatial resolution = 1.7–3.1 × 1.7–3.1 × 2.2–3.3 mm, temporal resolution = 38.4–43.2 ms (13–30 cardiac time frames), TE/TR = 2.32–2.85/4.8–5.4 ms, flip angle = 7°−15°, and velocity encoding = 150–250 cm/s (selected for each subject by the technologist to avoid velocity aliasing). Each subject also underwent breath-held 2D balanced SSFP cine MRI in short-axis orientation (base to apex) with spatial resolution = 1.0 × 1.0 × 6.0–2.2 × 2.2 × 8.0 mm^3, FOV = 243 × 276 × 150–420 × 420 × 170 mm^3, spacing between slices = 8–10 mm, temporal resolution = 27.1–40.6 ms (25–40 cardiac time points), TE/TR = 1.07–1.16/2.1–3.1 ms, and flip angle = 30°−75°.

2.3 | Data analysis

The data-analysis workflow for this study is shown in Figure 1. All code used for the WSS calculation and Atlas generation is freely available (https://github.com/alexbarks/atlas-tool). The 4D-flow data preprocessing was carried out using custom software in *MATLAB* (MathWorks, Natick, MA) to correct for eddy currents, Maxwell terms, and velocity aliasing as described previously.[17] The 4D-flow data were used to generate 3D phase-contrast MR angiograms, which were used for semi-automatic 3D segmentation of the thoracic aorta using commercial software (*MIMICS*; Materialise, Leuven, Belgium). A Laplacian filter was used to smooth the segmentation.[18]

2.3.1 | Systolic velocity and 3D-WSS calculation—For each subject, 4D-flow data were preprocessed to correct for eddy currents, velocity aliasing, and noise, and a phase-contrast MR angiogram was generated. A 3D segmentation of the aorta was generated semi-automatically (*MIMICS*) from the phase-contrast MR angiogram and used to mask the 4D-flow velocity. Peak systole was identified as the cardiac phase with the highest average velocity within the masked region, peak systolic velocities were stored for later analysis. Next, peak systolic 3D-WSS was calculated over the entire aorta surface at the peak systolic timepoint as described previously.[19] Briefly, at each surface point in the aorta segmentation, the coordinate system was transformed to have the z-direction match the inward normal, and velocity along the z-direction was assumed to be zero. One-dimensional smoothing splines were fit to the velocity data in each direction in the plane perpendicular to the inward normal vector, and the resulting 3D-WSS vector was transformed back into the original coordinate system.

2.3.2 | Helicity calculation—Preprocessed systolic velocity data were masked and used to calculate the helicity, $H = \int \vec{v} \cdot (\nabla \times \vec{v}) dV$, where $\vec{v}$ is the velocity vector at each voxel in each subject. Helicity values are reported as the median of the positive values and the median of the negative values, to show the presence of complex helical flow even when the overall mean is near zero.

2.3.3 | Aorta diameter calculation—A smoothed surface mesh was generated from each manual segmentation, and a normal vector to each triangulated surface feature was calculated. The distance along this normal vector to the next surface was calculated and averaged over the corresponding triangulated surface to approximate the diameter over the entire aorta surface.[20]

2.3.4 | Systolic velocity and 3D-WSS atlases—As detailed in a previous publication,[11] group-averaged systolic 3D-WSS and velocity atlases were generated using a four-step process. First, a group of interest was identified; in this study, the groups were either age and sex matched or only age matched. Second, the thoracic aorta segmentations of each subject in the group were co-registered using affine registration to a randomly selected member of the group, and an “overlap map” quantifying overlapping aorta geometry was generated. Third, a threshold minimizing the registration error was applied to the overlap map to generate the optimal group-averaged aorta geometry. Finally, 3D-WSS and peak-velocity data from each subject were mapped to the optimal group-averaged geometry (peak

systolic velocities mapped throughout the aorta volume, 3D-WSS mapped to the aorta surface). At each voxel within the optimal group-averaged aorta geometry, the mean and SD of the velocity were calculated, and at each surface point the mean and SD of the 3D-WSS were calculated. This resulted in a group-averaged 3D-WSS and velocity atlas, reflecting the normal physiologic mean velocity and 3D-WSS for the group at peak systole, as well as the normal variation within the group. Affine registration for steps 2 and 4 was carried out using FMRIB's Linear Image Registration Tool (FLIRT).[21]

2.3.5 | Velocity, 3D-WSS, helicity, and diameter comparison between groups—Systolic velocity and 3D-WSS were compared between groups to assess differences due to age and sex. For each age group (18–30, 31–40, 41–50, 51–60, and 61–80 years), the atlas of males was compared with the atlas of females of the same age. To compare across different age groups, atlases of each age group were compared with those in neighboring age groups (ie, the 31–40-year-old atlas was compared with the 18–30-year-old atlas and the 41–50-year-old atlas). To compare 3D-WSS and velocity values between groups, subjects in one group were registered using affine registration to the atlas of the second group, and the transformation matrix was applied to the 3D-WSS and velocity vector data for each subject to generate an atlas for the first group using the idealized geometry of the second. To check for consistency, for each comparison the registration procedure was carried twice (once while fixing the first atlas and registering the second group to it, and once while fixing the second atlas and registering the first group to it) and percent volume/area where the velocity/3D-WSS two groups differed was compared.

As diagrammed in Figure 1B, regional analysis of the mean and maximum systolic velocity, mean and maximum 3D-WSS, and median diameter was conducted by manually placing planes along the aorta midline to divide the segmentation for each subject into ascending aorta (AAo), aortic arch, and descending aorta (DAo). Planes were positioned at the takeoff of the innominate artery (AAo to arch) and immediately distal to the left subclavian artery (arch to DAo); example planes are shown in Figure 1B. The maximum velocity was filtered to avoid noise by sorting the velocity magnitude values in the region, calculating the average slope of the top 1% of the sorted velocity magnitude values, and ignoring voxels where the slope exceeds 10 times the mean.[22] To mitigate the influence of noise in the maximum 3D-WSS measurement, the 3D-WSS maximum is reported as the 98th percentile of the sorted 3D-WSS magnitude for the region. Helicity is reported as the median positive helicity value and the median negative helicity value in the region to avoid showing near-zero helicity in regions where high positive and negative helicities cancel out.

2.3.6 | Global left-ventricular function—Left-ventricular function metrics were measured by importing short-axis balanced SSFP cine images and manually drawing contours at peak systole and end diastole (Circle cvi[42]; Circle Cardiovascular Imaging, Calgary, Canada). For each subject, end-diastolic volume (EDV), end-systolic volume (ESV), ejection fraction (EF), stroke volume (SV), and cardiac output were calculated. The myocardial mass was measured at diastole. Left-ventricular volume and mass metrics as well as diameter were normalized by body surface area (BSA), calculated using the Mosteller method.[23]

2.4 | Statistical methods

To compare velocity differences across atlases, a Mann-Whitney U test was applied at each voxel within the aorta after registration with significance at $P < .05$. Velocity P-value maps were generated showing volumes where the velocity differed significantly between atlas groups. To compare 3D-WSS between atlases, a similar procedure was carried out, and a Mann-Whitney U test was used at each surface point after mapping both groups being tested to a shared geometry to test significance at $P < .05$. P-value maps were generated by displaying all surface points where the groups were significantly different.

For metrics that were measured for each subject (left ventricular function metrics, peak/mean regional velocity, peak/mean regional 3D-WSS, and median diameter), Pearson correlation coefficients and P-values were calculated to investigate correlations between left ventricular function metrics and aorta velocity and 3D-WSS, as well as velocity and 3D-WSS and age. Correlations were considered significant if $P < .05$. Normality was assessed by a Shapiro-Wilk test with $\alpha = .05$, medians are reported for non-normal distributions.

For comparisons between groups of subjects, an ANOVA (normally distributed data) or Kruskal-Wallis test (non-normally distributed data) was used. If a significant result was obtained, pairwise comparisons were carried out with Bonferroni correction using a t test (normally distributed data) or Mann-Whitney U test (non-normally distributed data).

3 | RESULTS

3.1 | Study population

Demographics, global cardiac function, and aorta diameters for the subject groups are given in Table 1, where data are reported in age groups of 18–30, 31–40, 41–50, 51–60, and 61–80 years old. When fitting a linear model, body mass index, height, weight, heart rate, cardiac output, and ejection fraction had no significant correlation with age. Normalized left ventricular EDV, ESV, and SV all significantly decreased with increasing age ($r = [-0.24]-[-0.28]$, $P = .005–.016$). In contrast, normalized myocardial mass increased with increased age ($r = 0.22$, $P = .24$). An increase in median diameter was associated with increased age in all three aorta segments, whether the value was unnormalized ($r > 0.55$, $P < .001$) or was normalized by BSA ($r > 0.36$, $P < .001$). Fitting a linear model to median diameter and age showed that the median diameter across our study population increased by 1.3 mm/decade in the AAo ($r^2 = 0.30$, $P < .001$), 1.1 mm/decade in the arch ($r^2 = 0.36$, $P < .001$), and 0.9 mm/decade in the DAo ($r^2 = 0.31$, $P < .001$) (Supporting Information Figure S1).

3.2 | Impact of age and sex on normal aortic velocity and 3D-WSS distribution

Subjects were placed into groups based on sex and age (18–30, 31–40, 41–50, 51–60, and 61–80 years), with 10 subjects in each group. Group-average systolic-velocity and 3D-WSS maps and corresponding P-value maps depicting regional sex differences in systolic velocity and 3D-WSS for all age groups are shown in Figure 2. The age- and sex-atlases are openly available for download with recognition given to funding sources given in this manuscript and refence to this manuscript (https://doi.org/10.18131/g3-knrk-5191). The largest sex-dependent differences were found in the 18- to 30-year-old group, in which males had

significantly higher 3D-WSS over 8% of the aorta surface area, and higher systolic velocity over 8% of the aorta volume. Significant variations were found over less than 1% of the aorta volume for systolic velocity and 5% or less of the aorta surface area for 3D-WSS in all other age groups. Changing the order in which subjects were registered had minimal effects on the comparison, with changes of less than 1% in the volume where systolic velocities differed and less than 1% in the area where 3D-WSS differed in all comparisons.

As differences due to sex were minor, subjects were placed into groups of 20 based solely on age (18–30, 31–40, 41–50, 51–60, and 61–80 years) for the remainder of the analysis. As shown in Figure 3, each age group was compared with the neighboring age groups (example: 31–40 years was compared with 18–30 years and 41–50 years) to assess changes in velocity and 3D-WSS during aging.

Systolic velocity increased in 1% or less of the aorta volume with increasing group age, whereas it significantly decreased in 13%, less than 1%, 7%, and 55% of the aorta volume between successively older groups (18–30 years, 31–40 years, 41–50 years, 51–60 years, and 61–80 years).

Similarly, Figure 4 shows the anterior and posterior views of the atlas 3D-WSS as well as *P*-value maps for comparisons between groups of sequential age. In all comparisons, 3D-WSS increased over less than 1% of the aorta surface area in the older group, whereas it decreased over 21%, 2%, 30%, and 62% of the aorta surface area in successively older groups.

3.3 | Regional aortic hemodynamics during aging

Trends in the peak and mean systolic velocity, helicity, and mean 3D-WSS for each aorta region during aging are summarized in Table 2. When fit with a linear model, increased subject age was associated with decreased mean velocity in the AAo ($r = -0.31$, $P = .001$), arch ($r = -0.56$, $P < .001$), and DAo ($r = -0.71$, $P < .001$), as well as decreased mean 3D-WSS in the AAo ($r = -0.33$, $P = .001$), arch ($r = -0.52$, $P < .001$), and DAo ($r = -0.73$, $P < .001$). Increased age was also associated with increased maximum systolic velocity in the AAo ($r = 0.25$, $P = .012$) and decreased maximum systolic velocity in the arch ($r = -0.50$, $P < .001$) and DAo ($r = -0.65$, $P < .001$) and decreased maximum 3D-WSS in the arch ($r = -0.32$, $P = .001$) and DAo ($r = -0.66$, $P < .001$). With increasing age, the median positive systolic helicity decreased in all three regions ($r < -0.32$, $P \leq .001$), whereas the median negative systolic helicity increased ($r > 0.27$, $P < .007$). Systolic helicity values for all patients are shown in Figure 5, along with the linear fit.

Regional hemodynamics were compared in a group-wise manner, as shown in Figure 6. All trends were significant ($P < .05$ on Kruskal-Wallis testing), except for the maximum velocity in the AAo and the maximum 3D-WSS in the AAo.

3.4 | Associations of left-ventricular function with aortic velocities, 3D-WSS, and helicity

Results of correlation analysis between ventricular function parameters and 4D-flow hemodynamic measures in each region (AAo, Arch, and DAo) are provided in Table 3. Increased left-ventricular cardiac output was associated with the elevated mean velocity ($r > 0.30$, $P < .01$) and 3D-WSS ($r > 0.29$, $P < .01$) in all regions, as well as increased maximum

systolic velocity in the arch ($r = 0.34$, $P < .001$) and DAo ($r > 0.29$, $P = .003$) and increased maximum 3D-WSS in the arch ($r = 0.31$, $P = .005$) and DAo ($r = 0.28$, $P = .005$). Increased cardiac output also correlated with increased positive systolic helicity in all regions ($r > 0.30$, $P < .01$) and with decreased negative systolic helicity in all regions ($r < -0.27$, $P < .01$). Increased mean velocity and mean 3D-WSS in the arch and DAo were also associated with increased normalized EDV ($r > 0.31$, $P < .005$), ESV ($r > 0.27$, $P < .01$), and SV ($r > 0.28$, $P < .01$). Increased maximum velocity in the arch and DAo were associated with increased normalized EDV ($r > 0.31$, $P < .002$), normalized ESV ($r > 0.27$, $P < .007$), and normalized SV ($r > 0.33$, $P < .001$). Increased maximum 3D-WSS in the aortic arch and DAo was associated with increased normalized EDV ($r > 0.26$, $P < .009$), normalized ESV ($r > 0.21$, $P < .04$), and normalized SV ($r = 0.26$, $P < .009$). Increased positive helicity in the arch and DAo was associated with increased normalized EDV, ESV, and SV ($r > 0.29$, $P < .01$). Similarly, decreased negative helicity in the arch and DAo was associated with increasing normalized EDV, ESV, and SV ($r < -0.29$, $P < .01$). Increased maximum systolic velocity in the AAo was associated with increased normalized myocardial mass ($r = 0.27$, $P = .007$). Increased heart rate was associated with an increased mean 3D-WSS in the AAo ($r = 0.22$, $P < .05$).

3.5 | Association between aorta diameter and mean velocity and 3D-WSS

The mean velocity and the mean 3D-WSS magnitude at systole for each region are shown plotted against the median regional diameter for each subject in Figure 7. In all three regions of the aorta, an increase in the median diameter of that region is associated with a decrease in both the mean velocity ($r = [-0.45]–[-0.52]$, $P < .001$) and mean 3D-WSS magnitude ($r = [-0.35]–[-0.56]$, $P < .001$) in that region.

4 | DISCUSSION

This study investigated changes in hemodynamics and cardiac function in the thoracic aorta due to aging and sex in a cohort of 100 healthy controls. We show that systolic velocity, 3D-WSS, and helicity in the aorta are strongly dependent on age, and velocity and 3D-WSS are less dependent on sex. Second, we found a significant decline in maximum systolic velocity, systolic helicity, and systolic 3D-WSS magnitude with age in the aortic arch and descending aorta, but an increase in maximum velocity and steady 3D-WSS in the ascending aorta with aging. Third, the decline in systolic velocity, helicity, and 3D-WSS is associated with an increasing diameter throughout the aorta as part of the aging process. Finally, in healthy controls, systolic velocity, helicity, and 3D-WSS are correlated with global left-ventricular function.

Using the atlas method, we showed the velocity and 3D-WSS in the aorta are strongly dependent on age, but that few differences exist between the sexes of the same age. One exception was found in the youngest age group (18–30 years), in which males had significantly higher systolic velocity and 3D-WSS than females of the same age in the ascending aorta. Furthermore, increasing velocity was found in focal regions corresponding to the level of the aortic valve for groups as age progressed from 31 to 60 years of age, possibly indicating increasing aortic valve sclerosis. This finding is supported by an

increasing maximum velocity in the AAo with age (Figure 6B) and can be seen regionally in Figure 3 with significantly elevated velocities at the level of the aortic valve. These results agree with the trends in a study of $N = 224$ normal aortas that found significant decreases in velocity and 3D-WSS in the thoracic aorta with age and no influence of sex on 3D-WSS.[14] Our data also extend this work to show no influence of sex on velocity, except in the youngest age group. This agrees with earlier work using 2D phase-contrast MRI that showed no significant difference between males and females in flow rate or mean 3D-WSS in the supraceliac and infrarenal levels of the descending aorta at rest and during exercise.[24] However, the earlier study was limited to 11 subjects (5 female) between 20 and 28 years old, whereas this study includes an order of magnitude more subjects and includes age stratification. Evidence from this current study shows that velocity and 3D-WSS similarities between males and females extend into the thoracic aorta for subjects greater than 30 years of age.

We also found significant decreases in both maximum systolic velocity and 3D-WSS in the arch and DAo with age, whereas the maximum systolic velocity in the ascending aorta increased with age and the maximum 3D-WSS was steady in the AAo. Positive and negative helicity magnitudes decreased in all regions of the aorta. Elevated velocities may explain a lack of change in the maximum 3D-WSS in the AAo despite decreases in the arch and DAo. We also replicated the findings of a trial in $N = 224$ patients without advanced cardiac disease using 4D-flow MRI,[14] which showed higher 3D-WSS in the descending aorta relative to the ascending aorta, although the values are not directly comparable, as the data in the earlier study were extensively preprocessed with a proprietary algorithm.[25] The previous work also highlighted the asymmetric distribution of 3D-WSS in the thoracic aorta, which can also be appreciated using 3D visualization, as seen in our data in Figure 4. The trends we found in systolic helicity mirror those found in an earlier study by Callaghan et al in $N = 247$ subjects without aortic or aortic valve pathology, in whom peak helicity decreased by 80%.[10] This study calculated helicity on six planes in the aorta, whereas we computed helicity in a volumetric manner and reported results for three regions. In contrast to these previous works, our study population consisted entirely of prospectively recruited healthy controls not referred for cardiovascular concerns and evenly distributed by age and sex. The atlas method also allowed for the concise comparison of both surface and volumetric quantities for visualization on the 3D aorta geometry, and division into regions of interest based on anatomic features. We demonstrated significant changes in velocity and 3D-WSS compared with prior 4D-flow repeatability testing in healthy controls with scans several weeks apart.[26] This work found coefficients of variation of 9% for velocity and 8% for 3D-WSS during regional analysis, whereas we found larger changes in the regional velocity and 3D-WSS except in the ascending aorta.

Additionally, we found that declines in systolic velocity, 3D-WSS, and helicity were associated with an increasing regional diameter with age. Although vessel distensibility is known to decrease with age,[27] which could contribute to increased 3D-WSS through faster flow accelerations and therefore systolic blood velocity gradients, 3D-WSS has also been found to strongly decrease with increasing vessel caliber,[28] counteracting this effect. We found that the median diameter increased between 0.9 and 1.3 mm/decade in our study, which agrees closely with other studies that have shown diameter increases in the ascending

aorta of about 1 mm per decade in the healthy population.[29–31] We also found that increasing diameter was significantly associated with decreasing velocity and 3D-WSS. We saw a decrease in the mean 3D-WSS in all aorta regions, even in the AAo, where the maximum 3D-WSS does not significantly change with age. We hypothesize that the diameter growth drives down the mean velocity and 3D-WSS in the AAo, whereas the increased velocity is limited to a jet potentially caused by an increasingly sclerotic aortic valve (see evidence in Figure 3, bottom row), confining the increased 3D-WSS regions to only a portion of the AAo wall, where the flow jet may impinge on the wall. Decreases in systolic velocity are also a major factor in decreasing the vorticity throughout the aorta.

Finally, we found that in healthy controls with normal left-ventricular function, systolic velocity, 3D-WSS, and helicity in the aorta were correlated with metrics of left-ventricular function. Our study replicated results from larger studies of left-ventricular function in subjects with no history of cardiovascular disease. Compared with the Multi-ethnic Study of Atherosclerosis trial ($N = 3015$), we found that EDV/BSA and SV/BSA decreased with aging.[2,3] However, we found slow increases in myocardial mass/BSA, whereas the Multi-ethnic Study of Atherosclerosis study showed slow decrease for all groups except risk-free females. This difference might be attributable to the larger cohort or additional risk stratification in the Multi-ethnic Study of Atherosclerosis trial compared with our study. The findings are especially important if these measurements are used in the future to risk-stratify individual patients, as proposed in previous pilot studies.[9] Finally, as cardiac output was correlated with 3D-WSS measures, future studies should further investigate the utility of normalizing 3D-WSS by cardiac output.

There are some limitations associated with MRI and 4D-flow acquisitions. The technique relies on time-consuming manual 3D segmentation of the aorta from generated phase-contrast MR angiograms (PCMRA), which remain to be optimized for the clinical workflow. Furthermore, the segmentations are weighted to represent the aorta geometry at systole (because the phase-contrast MR angiogram intensity is weighted by velocity); thus, we have limited our analysis to investigate only systolic velocity, helicity, and 3D-WSS. Focusing on peak systole precluded the calculation of time-averaged 3D-WSS or oscillatory shear index. Limited spatial resolution is also known to result in underestimation of 3D-WSS.[32,33] However, the subjects in this study were measured using the same technique at similar resolutions, which allows for the comparison of relative 3D-WSS within this study. Future work could use a more uniform MRI protocol at a single field strength to reduce variability due to differences in resolution and encoding velocity and could include healthy controls scanned using hardware from different vendors. The atlases were computed using affine registration, which results in some errors due to imperfect registration. Future studies could explore generating the atlases using a deformable registration. Future studies could further increase the study recruitment, as the number of subjects in each age group were still small ($N = 10$) compared with studies of left-ventricular function. Expansion of the study population could also include pediatric subjects and improve stratification of our eldest age group, although recruiting geriatric subjects without any history of cardiovascular disease can be challenging. Future studies could also examine the effects of medications and subject blood pressure on the hemodynamics of healthy aortas and examine the lack of changes in

systolic velocity and 3D-WSS in subjects between 31 and 50 years old, and could add additional metrics such as pulse wave velocity.

5 | CONCLUSIONS

Aortic hemodynamics depend strongly on age and less strongly on sex. When comparing velocity, 3D-WSS, or helicity of patients with aortic disease to groups of healthy controls, age-matched groups should be used. Furthermore, systolic aortic velocity, 3D-WSS, and helicity demonstrate some level of correlation with left-ventricular function; care should be taken if these factors are not controlled for. Normative values for velocity and 3D-WSS from healthy populations enable the quantitative determination of where regions in patients with aortic disease exceed specific confidence intervals. These results may aid in clinical management and risk stratification of these patients in the future.

Supplementary Material

Refer to Web version on PubMed Central for supplementary material.

Funding information

National Heart, Lung, and Blood Institute, Grant/Award Number: F30HL145995, K25HL119608, R01HL115828 and R01HL133504; National Institutes of Health, Grant/Award Number: T32GM008152

REFERENCES

1. Cain PA, Ahl R, Hedstrom E, et al. Age and gender specific normal values of left ventricular mass, volume and function for gradient echo magnetic resonance imaging: a cross sectional study. BMC Med Imaging. 2009;9:2. [PubMed: 19159437]
2. Cheng S, Fernandes VR, Bluemke DA, McClelland RL, Kronmal RA, Lima JA. Age-related left ventricular remodeling and associated risk for cardiovascular outcomes: the Multi-Ethnic Study of Atherosclerosis. Circ Cardiovasc Imaging. 2009;2:191–198. [PubMed: 19808592]
3. Liu CY, Lai S, Kawel-Boehm N, et al. Healthy aging of the left ventricle in relationship to cardiovascular risk factors: the Multi-Ethnic Study of Atherosclerosis (MESA). PLoS ONE. 2017;12:e0179947. [PubMed: 28640873]
4. Markl M, Frydrychowicz A, Kozerke S, Hope M, Wieben O. 4D flow MRI. J Magn Reson Imaging. 2012;36:1015–1036. [PubMed: 23090914]
5. Hope MD, Meadows AK, Hope TA, et al. Clinical evaluation of aortic coarctation with 4D flow MR imaging. J Magn Reson Imaging. 2010;31:711–718. [PubMed: 20187217]
6. Wigstrom L, Sjoqvist L, Wranne B. Temporally resolved 3D phase-contrast imaging. Magn Reson Med. 1996;36:800–803. [PubMed: 8916033]
7. Garcia J, Barker AJ, Murphy I, et al. Four-dimensional flow magnetic resonance imaging-based characterization of aortic morphometry and haemodynamics: impact of age, aortic diameter, and valve morphology. Eur Heart J Cardiovasc Imaging. 2016;17:877–884. [PubMed: 26377908]
8. Malek AM, Alper SL, Izumo S. Hemodynamic shear stress and its role in atherosclerosis. JAMA. 1999;282:2035–2042. [PubMed: 10591386]
9. Guzzardi DG, Barker AJ, van Ooij P, et al. Valve-related hemodynamics mediate human bicuspid aortopathy: insights from wall shear stress mapping. J Am Coll Cardiol. 2015;66:892–900. [PubMed: 26293758]
10. Callaghan FM, Bannon P, Barin E, et al. Age-related changes of shape and flow dynamics in healthy adult aortas: a 4D flow MRI study. J Magn Reson Imaging. 2019;49:90–100. [PubMed: 30102443]

11. van Ooij P, Potters WV, Nederveen AJ, et al. A methodology to detect abnormal relative wall shear stress on the full surface of the thoracic aorta using four-dimensional flow MRI. Magn Reson Med. 2015;73:1216–1227. [PubMed: 24753241]
12. van Ooij P, Potters WV, Collins J, et al. Characterization of abnormal wall shear stress using 4D flow MRI in human bicuspid aortopathy. Ann Biomed Eng. 2015;43:1385–1397. [PubMed: 25118671]
13. van Ooij P, Garcia J, Potters WV, et al. Age-related changes in aortic 3D blood flow velocities and wall shear stress: implications for the identification of altered hemodynamics in patients with aortic valve disease. J Magn Reson Imaging. 2016;43:1239–1249. [PubMed: 26477691]
14. Callaghan FM, Grieve SM. Normal patterns of thoracic aortic wall shear stress measured using four-dimensional flow MRI in a large population. Am J Physiol Heart Circ Physiol. 2018;315:H1174–H1181. [PubMed: 30028202]
15. Marwick TH, Gillebert TC, Aurigemma G, et al. Recommendations on the use of echocardiography in adult hypertension: a report from the European Association of Cardiovascular Imaging (EACVI) and the American Society of Echocardiography (ASE). Eur Heart J Cardiovasc Imaging. 2015;16:577–605. [PubMed: 25995329]
16. Markl M, Harloff A, Bley TA, et al. Time-resolved 3D MR velocity mapping at 3T: improved navigator-gated assessment of vascular anatomy and blood flow. J Magn Reson Imaging. 2007;25:824–831. [PubMed: 17345635]
17. Bock J, Kreher BW, Hennig J, Markl M. Optimized pre-processing of time-resolved 2D and 3D phase contrast MRI data. Proc Int Soc Magn Reson Med. 2007;15:3138.
18. Vollmer J, Mencl R, Müller H. Improved Laplacian smoothing of noisy surface meshes. Eurographics. 1999;18:131–138.
19. Potters WV, van Ooij P, Marquering H, vanBavel E, Nederveen AJ. Volumetric arterial wall shear stress calculation based on cine phase contrast MRI. J Magn Reson Imaging. 2015;41:505–516. [PubMed: 24436246]
20. van Ooij P, Collins J, Fedak PW, et al. 3D linear regression analysis reveals relationships of 4D flow MRI-derived aortic dimensions with age, gender and wall shear stress in patients with aortopathy In: Proceedings of the 25th Annual Meeting of ISMRM, Honolulu, Hawaii, 2017 p. 288.
21. Jenkinson M, Smith S. A global optimisation method for robust affine registration of brain images. Med Image Anal. 2001;5:143–156. [PubMed: 11516708]
22. Rose MJ, Jarvis K, Chowdhary V, et al. Efficient method for volumetric assessment of peak blood flow velocity using 4D flow MRI. J Magn Reson Imaging. 2016;44:1673–1682. [PubMed: 27192153]
23. Mosteller RD. Simplified calculation of body-surface area. N Engl J Med. 1987;317:1098. [PubMed: 3657876]
24. Cheng CP, Herfkens RJ, Taylor CA. Comparison of abdominal aortic hemodynamics between men and women at rest and during lower limb exercise. J Vasc Surg. 2003;37:118–123. [PubMed: 12514587]
25. Callaghan FM, Grieve SM. Spatial resolution and velocity field improvement of 4D-flow MRI. Magn Reson Med. 2017;78:1959–1968. [PubMed: 27885707]
26. van Ooij P, Powell AL, Potters WV, Carr JC, Markl M, Barker AJ. Reproducibility and interobserver variability of systolic blood flow velocity and 3D wall shear stress derived from 4D flow MRI in the healthy aorta. J Magn Reson Imaging. 2016;43:236–248. [PubMed: 26140480]
27. Mohiaddin RH, Firmin DN, Longmore DB. Age-related changes of human aortic flow wave velocity measured noninvasively by magnetic resonance imaging. J Appl Physiol (1985). 1993;74:492–497. [PubMed: 8444734]
28. Truong U, Fonseca B, Dunning J, et al. Wall shear stress measured by phase contrast cardiovascular magnetic resonance in children and adolescents with pulmonary arterial hypertension. J Cardiovasc Magn Reson. 2013;15:81. [PubMed: 24034144]
29. Turkbey EB, Jain A, Johnson C, et al. Determinants and normal values of ascending aortic diameter by age, gender, and race/ethnicity in the Multi-Ethnic Study of Atherosclerosis (MESA). J Magn Reson Imaging. 2014;39:360–368. [PubMed: 23681649]

30. Devereux RB, de Simone G, Arnett DK, et al. Normal limits in relation to age, body size and gender of two-dimensional echocardiographic aortic root dimensions in persons ≥15 years of age. Am J Cardiol. 2012;110:1189–1194. [PubMed: 22770936]

31. Davis AE, Lewandowski AJ, Holloway CJ, et al. Observational study of regional aortic size referenced to body size: production of a cardiovascular magnetic resonance nomogram. J Cardiovasc Magn Reson. 2014;16:9. [PubMed: 24447690]

32. Stalder AF, Russe MF, Frydrychowicz A, Bock J, Hennig J, Markl M. Quantitative 2D and 3D phase contrast MRI: optimized analysis of blood flow and vessel wall parameters. Magn Reson Med. 2008;60:1218–1231. [PubMed: 18956416]

33. Petersson S, Dyverfeldt P, Ebbers T. Assessment of the accuracy of MRI wall shear stress estimation using numerical simulations. J Magn Reson Imaging. 2012;36:128–138. [PubMed: 22336966]

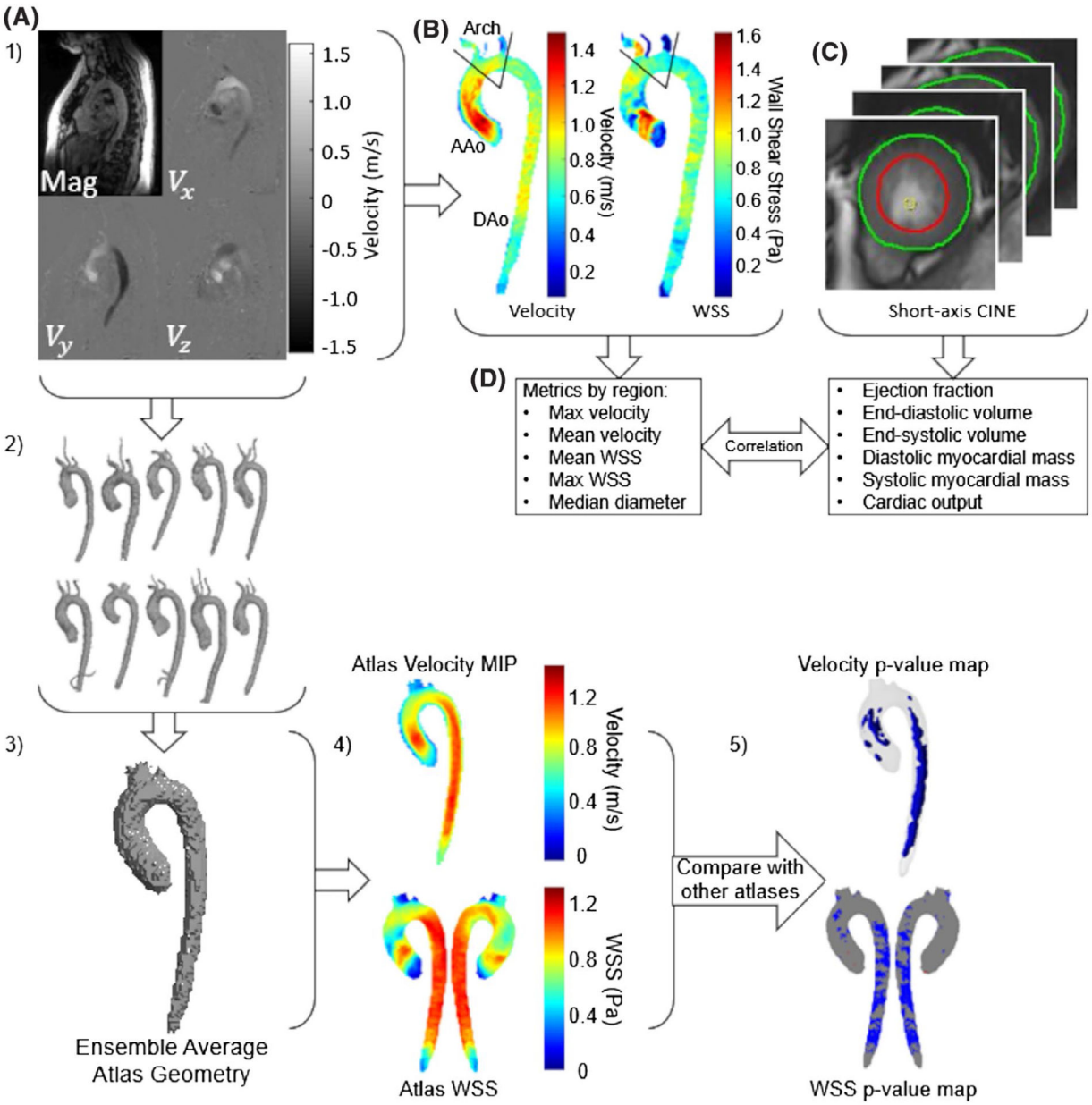

FIGURE 1.

Global function and hemodynamic correlations. A, Four-dimensional flow MRI data were preprocessed and a manual 3D segmentation of the aorta was generated. B, Velocity information was used to calculate 3D wall shear stress (3D-WSS) on the entire surface of the aorta. The aorta was divided into three segments (ascending aorta [AAo], arch, and descending aorta [DAo]) by placing planes before the takeoff of the innominate artery and after the left subclavian artery, and hemodynamic parameters were calculated for each region. C, Endocardial and epicardial contours were drawn at peak systole and end diastole on short-axis images to extract left-ventricular function metrics. D, Velocity and 3D-WSS values from the 4D flow were correlated with the left-ventricular function metrics from the short-axis cine images. 1–5, Age/sex-stratified hemodynamic atlas comparison: (1) The

same 4D-flow MRI data and manual 3D segmentations were used. (2) A cohort of $N = 10$ subjects (sex comparisons) or $N = 20$ subjects (age comparisons) were assembled. (3) An ensemble average atlas geometry was calculated for the cohort. (4) Average velocity (shown here as a maximum intensity projection [MIP]) and 3D-WSS (shown as a color-mapped surface) were calculated for the cohort. (5) Velocity and 3D-WSS were compared between different cohorts to generate P-value maps showing where the velocity and 3D-WSS differed significantly between cohorts (showing $P < .05$)

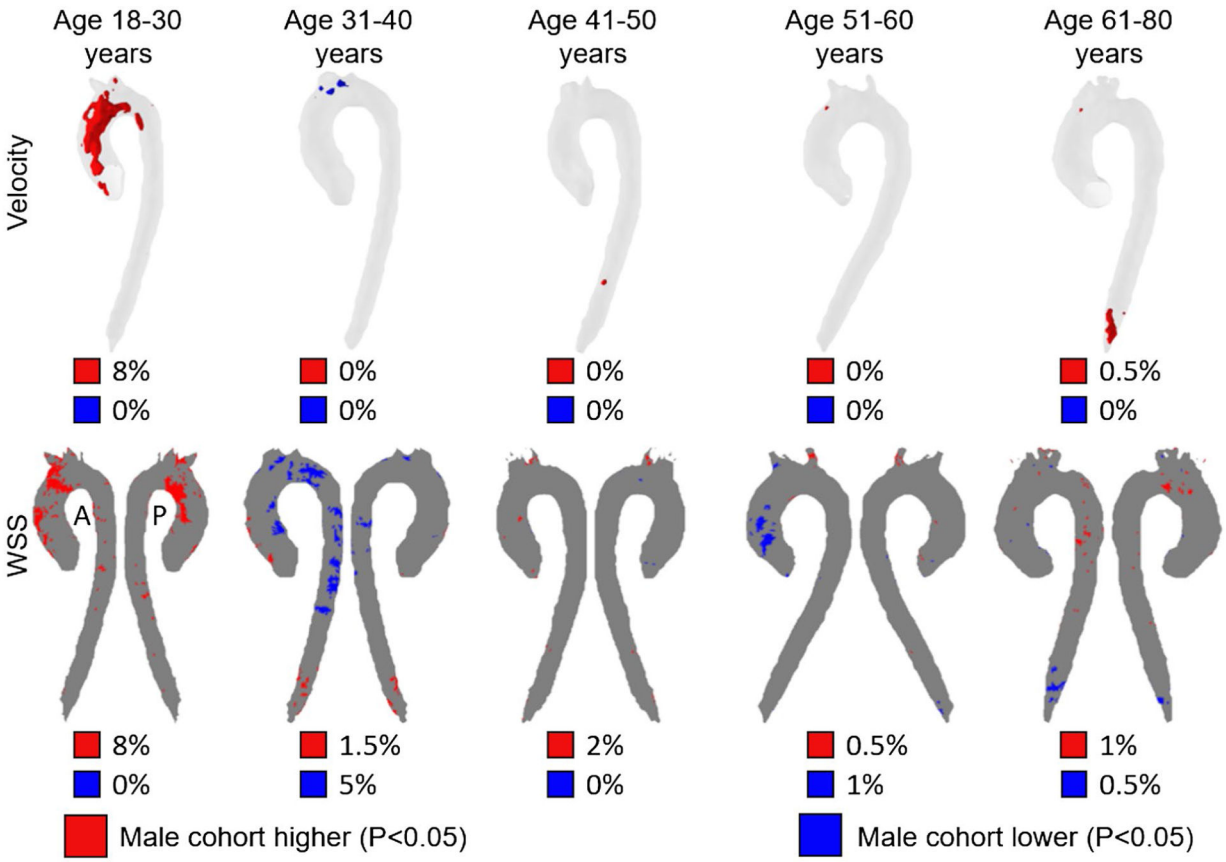

FIGURE 2.

Top row: Voxel-wise *P*-value maps showing voxels where velocity was significantly different ($P < .05$) between male and female cohorts of the same age. The percentiles below each *P*-value map indicate the fraction of the aorta volume where the male cohort has decreased (blue) or increased (red) velocities compared with the female cohort. Bottom row: *P*-value maps for 3D-WSS, showing points on the surface of the aorta where the 3D-WSS was significantly different between male and female cohorts of the same age ($P < .05$). The percentiles below each *P*-value map indicate the fraction of the aorta surface area where the male cohort has decreased (blue) or increased (red) 3D-WSS compared with the female cohort

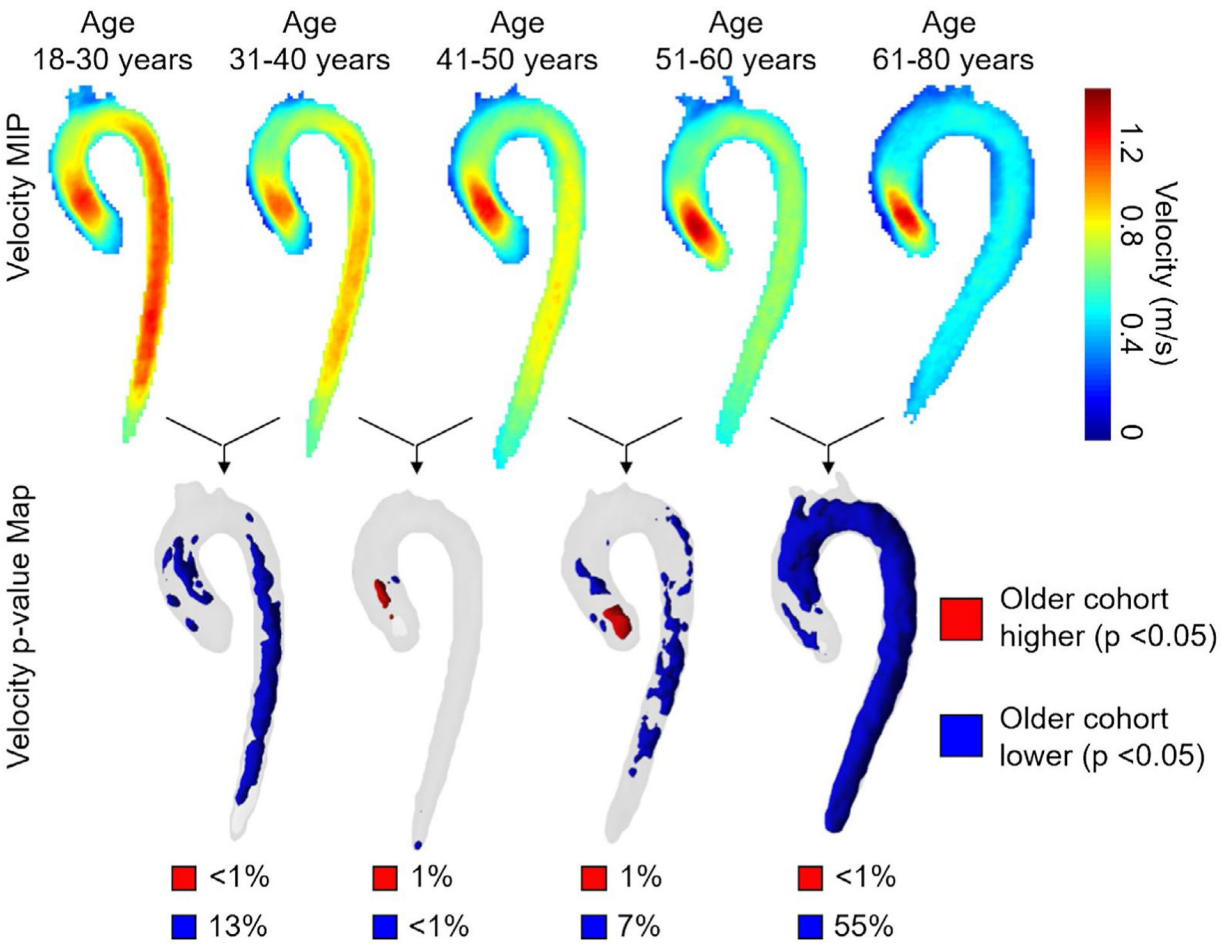

FIGURE 3.

Top row: Side-by-side comparisons of systolic velocity atlases (velocity MIPs) for each cohort of 20 age-stratified controls (10 males + 10 females in each group). For each age group, the atlas geometry was determined independently by registration of the 20 aortas. An age-dependent reduction of aorta systolic velocities can clearly be appreciated. Bottom row: Voxel-wise *P*-value maps calculated by pairwise registering the older to the younger cohort. Regions in blue/red show aorta regions with significantly lower/higher velocity ($P < .05$). The percentiles below each *P*-value map indicate the fraction of the aorta volume with decreased (blue) or increased (red) velocities compared with the younger cohort

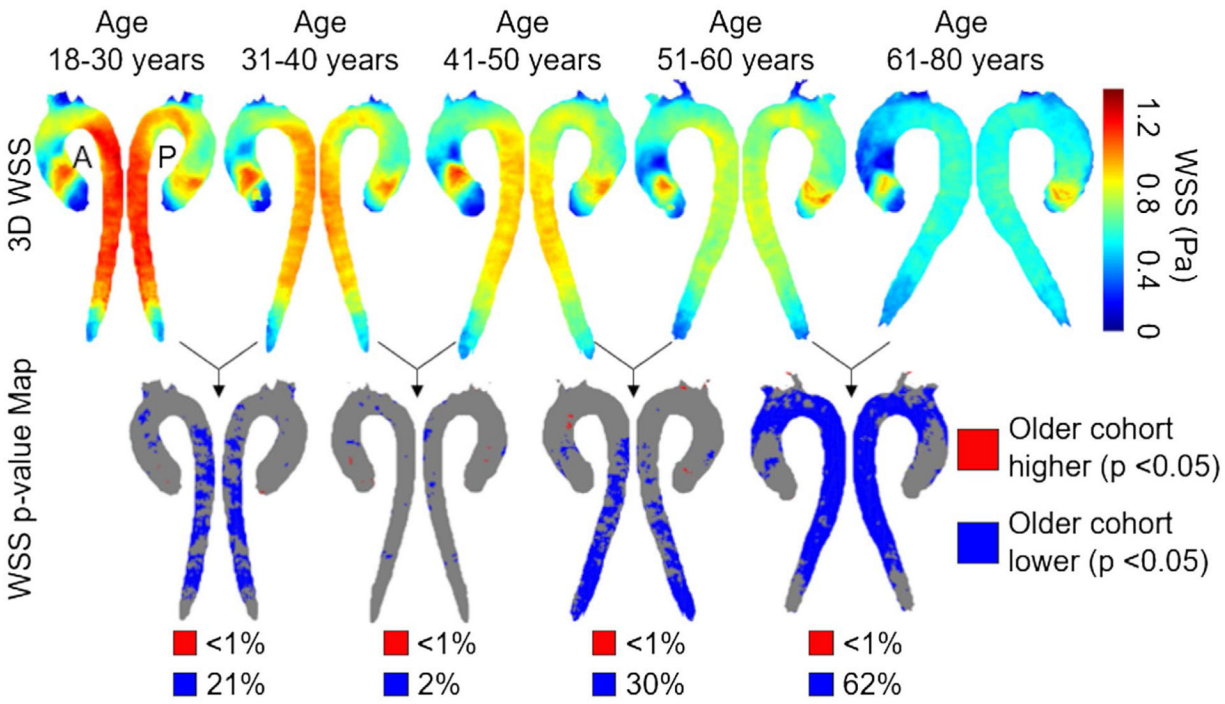

FIGURE 4.

Top row: Side-by-side comparisons of systolic 3D-WSS atlases for each cohort of 20 age-stratified controls (10 males + 10 females), with the anterior view on the left and the posterior view on the right. For each age group, the atlas geometry was independently determined by registration of the 20 aortas. Bottom row: *P*-value maps at each point on the aorta surface calculated pair-wise by registering the older cohort to the younger cohort. Regions in blue/red show aorta regions with significantly lower/higher 3D-WSS ($P < .05$). The percentiles below each *P*-value map indicate the fractions of the aorta surface area with decreased (blue) or increased (red) velocities compared with the younger cohort

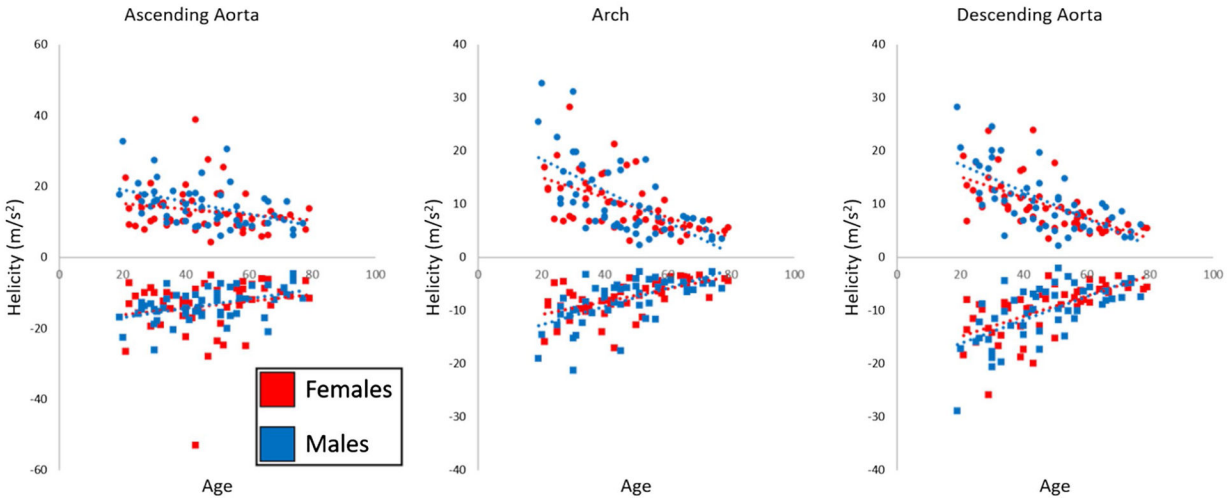

FIGURE 5.

Regional systolic helicity in all $N = 100$ healthy controls. Red markers indicate females, whereas blue markers indicate males, with circles showing the median positive helicity in the region and squares showing the median negative helicity in the region for each subject. Dashed lines indicating a linear fit show decreasing systolic helicity magnitude with age for both sexes

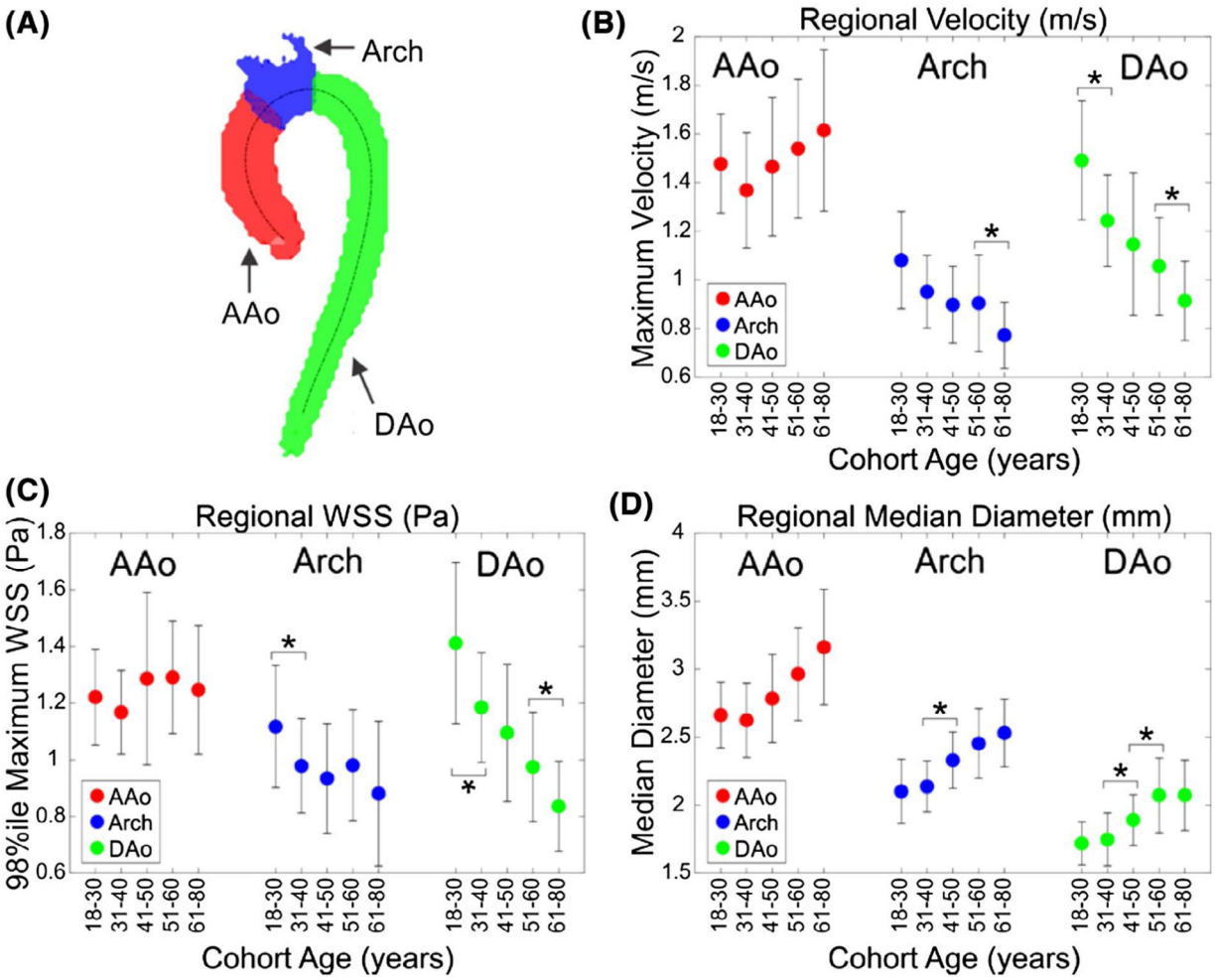

FIGURE 6.

Example aorta divided into three regions. Regional analysis (A) of systolic velocity (B), 3D-WSS (C), and median diameter (D) in the AAo, arch, and DAo by age. Each marker represents the mean of $N = 20$ subjects (10 female and 10 male), with error bars showing ±1 SD from the mean. The x-axis shows the cohort age in years. An asterisk (*) denotes a significant difference between neighboring age groups using Mann-Whitney U test with $\alpha = 0.05$. All trends were significant by Kruskal-Wallis testing except for AAo maximum velocity and AAo maximum 3D-WSS

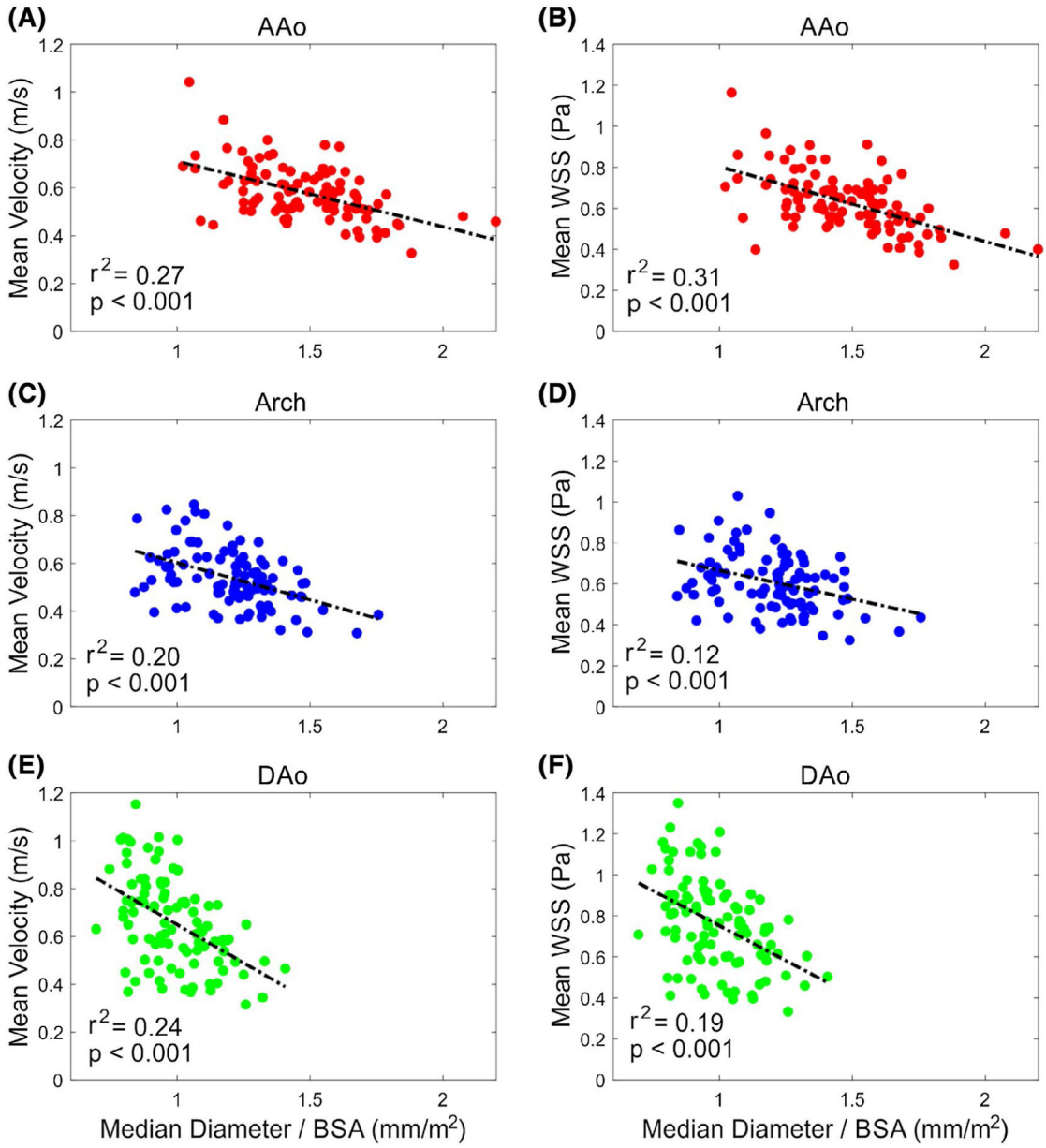

FIGURE 7.

Increasing diameter in each aortic region is associated with decreasing mean velocity and mean 3D-WSS magnitude in that region. Mean velocity in the AAo (A), arch (C), and DAo (E) decreases as the normalized median diameter of the region increases. The mean 3D-WSS in the AAo (B), arch (D), and DAo (F) also decreases with increased normalized median regional diameter. Each point represents 1 subject ($N = 100$ per plot); the dashed line shows a linear fit, with the associated r^2 value and P-value also shown on the plot. Abbreviation: BSA, body surface area

TABLE 1

Cohort demographics

	18–30 years	31–40 years	41–50 years	51–60 years	61–80 years	r	*P*-value	Trend
Age	25.9 ± 3.6	35.8 ± 3.2	45.4 ± 3.0	55.0 ± 2.8	68.9 ± 5.6	-	-	-
BMI	26.5 ± 5.5	27.6 ± 5.7	25.7 ± 4.8	26.9 ± 3.5	29.1 ± 5.1	0.15	.143	-
Height (m)	1.7 ± 0.1	1.7 ± 0.1	1.7 ± 0.1	1.7 ± 0.1	1.7 ± 0.1	0.03	.766	-
Weight (kg)	78.3 ± 19.4	79.4 ± 18.3	76.0 ± 17.1	78.0 ± 10.8	86.3 ± 19.4	0.140	.164	-
HR (BPM)	63.6 ± 8.1	66.5 ± 11	63.9 ± 10.8	67.7 ± 12	63 ± 11.4	−0.01	.921	-
CO (L/min)	5.5 ± 1.5	4.9 ± 0.9	5.1 ± 0.8	5.1 ± 1.1	4.7 ± 1	−0.16	.105	-
EF (%)	55.6 ± 4.5	55.8 ± 6.1	57.3 ± 3.7	57 ± 5.8	57 ± 6.3	0.11	.289	-
EDV / BSA (ml/m^2)	80.9 ± 14.4	70.2 ± 12.9	75.3 ± 11.3	69.6 ± 11.9	66.6 ± 15	−0.28	.005	↓
ESV / BSA (ml/m^2)	36.1 ± 8.2	31.3 ± 8	32.3 ± 6.7	30.1 ± 7.4	29.0 ± 8.9	−0.25	.011	↓
SV / BSA (ml/m^2)	44.8 ± 7.7	38.9 ± 7.5	42.9 ± 5.7	39.5 ± 6.9	37.6 ± 8.1	−0.24	.016	↓
Myocardial mass / BSA (g/m^2)	52.4 ± 9.9	47.6 ± 6.4	52.7 ± 8.4	52.1 ± 8.4	56.6 ± 11.8	0.22	.024	↑
AAo Median Diameter (mm)	26.6 ± 2.4	26.2 ± 2.7	27.8 ± 3.2	29.6 ± 3.4	31.6 ± 4.3	0.55	<.001	↑
Arch Median Diameter (mm)	21.0 ± 2.4	21.4 ± 1.9	23.3 ± 2.1	24.5 ± 2.6	25.3 ± 2.5	0.60	<.001	↑
DAo Median Diameter (mm)	17.2 ± 1.6	17.5 ± 1.9	18.9 ± 1.9	20.7 ± 2.7	20.7 ± 2.6	0.55	<.001	↑
AAo Median Diameter / BSA (mm/m^2)	14.1 ± 1.8	13.7 ± 1.7	14.9 ± 2.4	15.5 ± 2.0	15.8 ± 2.3	0.36	<.001	↑
Arch Median Diameter / BSA (mm/m^2)	11.1 ± 1.7	11.2 ± 1.4	12.5 ± 2.0	12.9 ± 1.5	12.6 ± 1.5	0.37	<.001	↑
DAo Median Diameter / BSA (mm/m^2)	9.1 ± 1.1	9.1 ± 0.9	10.1 ± 1.5	10.9 ± 1.6	10.3 ± 1.3	0.40	<.001	↑

Note: Cohort demographic information and left-ventricular function metrics are presented as the mean ± SD. Each age group includes 10 males and 10 females. Gray rows indicate those with significant Pearson coefficients ($P < .05$). The median diameter in each aorta region is shown as both raw values and normalized by BSA. The significance of the Pearson correlation coefficient (r) is presented in the *P*-value column.

Abbreviations: BMI, body mass index; CO, cardiac output; EDV/BSA, end-diastolic volume normalized by BSA; EF, ejection fraction; ESV/BSA, end-systolic volume normalized by BSA; HR, heart rate; SV/BSA, stroke volume normalized by BSA.

TABLE 2

Hemodynamic metrics during aging

	18–30 years	31–40 years	41–50 years	51–60 years	61–80 years	r	*P*-value	Trend
AAo Mean Velocity (m/s)	0.62 ± 0.12	0.58 ± 0.08	0.61 ± 0.15	0.58 ± 0.10	0.51 ± 0.09	−0.31	.001	↓
Arch Mean Velocity (m/s)	0.62 ± 0.13	0.58 ± 0.09	0.54 ± 0.12	0.52 ± 0.10	0.43 ± 0.06	−0.56	<.001	↓
DAo Mean Velocity (m/s)	0.83 ± 0.16	0.73 ± 0.13	0.68 ± 0.16	0.58 ± 0.12	0.45 ± 0.08	−0.71	<.001	↓
AAo Vmax (m/s)	1.48 ± 0.2	1.37 ± 0.24	1.46 ± 0.28	1.54 ± 0.28	1.61 ± 0.33	0.25	.012	↑
Arch Vmax (m/s)	1.08 ± 0.2	0.95 ± 0.15	0.9 ± 0.16	0.9 ± 0.2	0.77 ± 0.14	−0.5	<.001	↓
DAo Vmax (m/s)	1.49 ± 0.24	1.24 ± 0.19	1.15 ± 0.29	1.06 ± 0.2	0.91 ± 0.16	−0.65	<.001	↓
AAo Mean 3D-WSS (Pa)	0.67 ± 0.14	0.65 ± 0.11	0.66 ± 0.18	0.63 ± 0.12	0.54 ± 0.11	−0.33	.001	↓
Arch Mean 3D-WSS (Pa)	0.70 ± 0.15	0.64 ± 0.11	0.60 ± 0.12	0.61 ± 0.12	0.48 ± 0.09	−0.52	<.001	↓
DAo Mean 3D-WSS (Pa)	0.99 ± 0.19	0.84 ± 0.15	0.79 ± 0.17	0.67 ± 0.15	0.51 ± 0.10	−0.73	<.001	↓
AAo WSSmax (Pa)	1.22 ± 0.17	1.17 ± 0.15	1.29 ± 0.3	1.29 ± 0.2	1.25 ± 0.23	0.11	.276	-
Arch WSSmax (Pa)	1.12 ± 0.22	0.98 ± 0.17	0.93 ± 0.19	0.98 ± 0.2	0.88 ± 0.26	−0.32	.001	↓
DAo WSSmax (Pa)	1.41 ± 0.28	1.19 ± 0.19	1.09 ± 0.24	0.98 ± 0.19	0.84 ± 0.16	−0.66	<.001	↓
AAo Median Positive Helicity (m/s^2)	164 ± 63	138 ± 39	149 ± 80	135 ± 65	106 ± 32	−0.32	.001	↓
AAo Median Negative Helicity (m/s^2)	−151 ± 53	−139 ± 38	−156±103	−134 ± 56	−100 ± 40	0.27	.007	↑
Arch Median Positive Helicity (m/s^2)	163 ± 81	119 ± 43	102 ± 56	79 ± 37	56 ± 15	−0.60	<.001	↓
Arch Median Negative Helicity (m/s^2)	−111±45	−91 ± 27	−80 ± 38	−67 ± 26	−46 ± 12	0.59	<.001	↑
DAo Median Positive Helicity (m/s^2)	164 ± 55	116 ± 40	101 ± 53	80 ± 30	61 ± 18	−0.64	<.001	↓
DAo Median Negative Helicity (m/s^2)	−154± 54	−118 ± 41	−95 ± 43	−81 ± 29	−60 ± 16	0.63	<.001	↑

Note: Changes in aorta hemodynamic parameters during aging are presented. Each age group includes 10 males and 10 females. Regional velocity and 3D-WSS values were measured for each of the 100 subjects (20 per age group) and correlated for this table. Maximum velocity was filtered as described in the Methods section, and maximum 3D-WSS values represent the 98% percentile of the 3D-WSS magnitude in each region. Values are reported as the mean ± SD. Gray rows indicate those with significant Pearson coefficients (r) ($P < .05$). The significance is indicated by the *P*-values.

TABLE 3

Left-ventricular function metrics and hemodynamic correlations

	HR (BPM)	CO (L/min)	EF (%)	EDV / BSA (ml/m^2)	ESV / BSA (ml/m^2)	SV / BSA (ml/m^2)	Myocardial mass / BSA (g/m^2)
AAo Mean Velocity (m/s)	0.18	0.40	−0.05	0.17	0.16	0.15	0.11
Arch Mean Velocity (m/s)	0.08	0.38	−0.07	0.31	0.27	0.28	0.04
DAo Mean Velocity (m/s)	−0.02	0.30	−0.06	0.37	0.31	0.35	−0.05
AAo Vmax (m/s)	0.00	0.15	0.03	0.07	0.04	0.08	0.27
Arch Vmax (m/s)	0.01	0.34	−0.06	0.31	0.27	0.28	0.11
DAo Vmax (m/s)	−0.02	0.29	−0.02	0.35	0.28	0.34	0.01
AAo Mean 3D-WSS (Pa)	0.22	0.32	−0.05	0.09	0.10	0.06	0.03
Arch Mean 3D-WSS (Pa)	0.06	0.38	−0.04	0.34	0.28	0.33	0.07
DAo Mean 3D-WSS (Pa)	0.00	0.29	−0.03	0.37	0.30	0.35	−0.07
AAo WSSmax (Pa)	0.18	0.16	0.03	−0.03	−0.03	−0.01	0.13
Arch WSSmax (Pa)	−0.02	0.31	0.00	0.26	0.21	0.26	0.11
DAo WSSmax (Pa)	−0.02	0.28	−0.02	0.37	0.29	0.36	−0.01
AAo Median Positive Helicity (m/s^2)	0.14	0.39	−0.07	0.21	0.19	0.18	0.11
AAo Median Negative Helicity (m/s^2)	−0.19	−0.32	−0.03	−0.12	−0.08	−0.13	0.01
Arch Median Positive Helicity (m/s^2)	0.08	0.35	−0.14	0.36	0.35	0.29	0.07
Arch Median Negative Helicity (m/s^2)	0.01	−0.27	0.15	−0.36	−0.35	−0.29	−0.03
DAo Median Positive Helicity (m/s^2)	0.01	0.30	−0.09	0.34	0.30	0.30	0.00
DAo Median Negative Helicity (m/s^2)	0.02	−0.28	0.10	−0.37	−0.33	−0.33	0.00

Note: Pearson correlation coefficients (*r*) are presented between left-ventricular function metrics and hemodynamic parameters (velocity, 3D-WSS) from 4D-flow MRI of the aorta, with all metrics calculated for each subject. Yellow entries signify $P < .05$, orange signify $P < .01$, and red signifies $P < .001$. Cardiac output is significantly correlated with velocity and 3D-WSS in all aorta regions, and the volume metrics (end-diastolic volume, end-systolic volume, and stroke volume) are significantly correlated with the velocity and 3D-WSS in the arch and DAo. To reduce the influence of noise, maximum velocity was filtered as described in the Methods section, and the maximum 3D-WSS is the 98th percentile of the 3D-WSS distribution in that region.